Theor Chem Account (2008) 120:533–542
DOI 10.1007/s00214-008-0432-9

REGULAR ARTICLE

Protein–protein recognition: a computational mutagenesis study of the MDM2–P53 complex

Irina S. Moreira · Pedro A. Fernandes · Maria J. Ramos

Received: 1 November 2007 / Accepted: 20 February 2008 / Published online: 26 March 2008

Abstract Protein P53 is involved in more than 50% of the human cancers and the P53–MDM2 complex is a target for anticancer drug design. It is possible to engineer small P53 mimics that would be expected to disrupt the P53–MDM2 complex, and release P53 to initiate cell-cycle arrest or apoptosis. These small peptides should bind to the functional epitopes of the protein–protein interface, and prevent the interaction between P53 and MDM2. Here, we apply an improved computational alanine scanning mutagenesis method, which allows the determination of the hot spots present in both monomers, P53 and MDM2, of three protein complexes (the P53-binding domain of human MDM2, its analogue from *Xenopus laevis*, and the structure of human MDM2 in complex with an optimized P53 peptide). The importance of the hydrogen bonds formed by the protein backbone has been neglected due to the difficulty of measuring experimentally their contribution to the binding free energy. In this study we present a computational approach that allows the estimation of the contribution to the binding free energy of the C=O and N–H groups in the backbone of the P53 and MDM2 proteins. We have noticed that the hydrogen bond between the HE1 atom of the hot spot Trp23 and the O atom of the residue Leu54, as well as the NH-pi hydrogen bond between the Ile57 and Met58 were observed in the Molecular dynamics simulation, and their contribution to the binding free energy measured. This study not only shows the reliability of the computational mutagenesis method to detect hot spots but also demonstrates an excellent correlation between the quantitative calculated binding free energy contribution of the C=O and N–H backbone groups of the interfacial residues and the qualitative values expected for this kind of interaction. The study also increases our understanding of the P53–MDM2 interaction.

Keywords Alanine scanning mutagenesis · MM-PBSA · Hot spot · Bindingfree energy · Protein-protein interface · Molecular mechanics · P53 · MDM2 · Mutagenesis · Backbone hydrogen bond

1 Introduction

Protein P53 is a tumor suppressor that binds to DNA and regulates the expression of several genes with a wide range of biological functions such as regulation, apoptosis, DNA repair, and differentiation [1,2]. Therefore, it maintains the genomic integrity of the cell. The P53 is implicated in more than 50% of human cancers [3]. Inactivation of P53 can be achieved by mutation, deletion or it can be a consequence of an overexpression of the MDM2 protein (the murine double-minute clone 2, more appropriately termed human double-minute clone 2, or HDM2) [4–6]. P53 and MDM2 form a negative auto-regulatory feedback loop in non tumor cells. P53 production is increased in response to cellular stress such as DNA damage, which leads to the stimulation of the expression of the MDM2 protein. In response, the oncoprotein MDM2 protein inhibits the P53 protein. This can be achieved with the binding of MDM2 to the transactivation domain of the P53 protein or with MDM2 acting as an ubiquitin ligase, promoting P53 degradation, or with an increase of the exportation of P53 [7–9]. Most of the mutations in the P53 protein are missense mutations leading to only an amino acid change. These mutations are non-random being

Contribution to the Nino Russo Special Issue.

I. S. Moreira · P. A. Fernandes · M. J. Ramos (✉)
REQUI*M*TE/Departamento de Química,
Faculdade de Ciências da Universidade do Porto,
Rua do Campo Alegre 687, 4169-007 Porto, Portugal
e-mail: mjramos@fc.up.pt

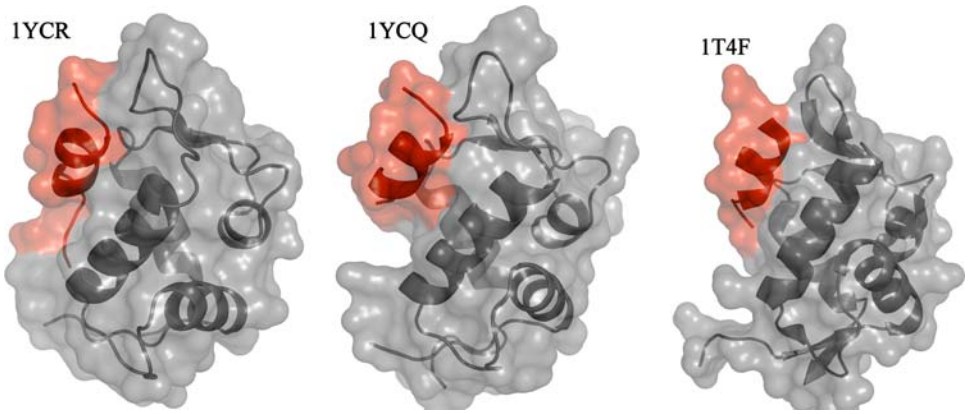

Fig. 1 Representation of complexes between the P53 protein (in *red*) and the MDM2 protein (in *grey*). X-ray crystallographic structures

essentially clusters in the central part of the molecule and 40% in the hot spot cluster [4–6].

Hence, the P53–MDM2 complex is a target for anticancer drug design [2]. It is possible to engineer small P53 mimics that are expected to disrupt the P53–MDM2 complex, and release P53 to initiate cell-cycle arrest or apoptosis. This small peptides bind to the protein-protein interface, and should prevent the interaction between P53 and MDM2 [2,10,11].

In Fig. 1a, b and c is represented the crystal structures of the P53-binding domain of human MDM2, hMDM2 (PDBID: 1YCR) [1], its analogue from *Xenopus laevis*, xMDM2 (PDBID: 1YCQ) [1] bound to the *N*-terminal of the human P53, and the structure of human MDM2 in complex with an optimized P53 peptide (PDBID: 1T4F) [12]. The first two complexes share 72.9% of amino acid sequence identity being this value even higher among the amino acid residues in the active site [12].

These complex interfaces are essentially constituted by hydrophobic and aromatic amino acid residues. Experimental and computational studies have identified three amino acids responsible for the majority of the binding free energy in the P53 protein (Phe19, Trp23, and Leu26) [1,13,14]. The Phe19/Trp23 of P53 is a good example of a Trp/Met/Phe cluster, which upon analysis of protein complexes using amino acid sequence order-independent multiple structural comparison algorithms, was shown to modulate protein function [15]. These three amino acid residues constitute a hot spot cluster. Hot spots have been defined as those sites where alanine mutations cause a significant increase in the binding free energy, of at least 2.0 kcal mol^{-1} [16,17]. Hot spots residues that are major contributors to the stability of the protein–protein complex have been shown to overlap with structurally conserved residues [18].

We have to make the distinction between structural epitopes (residues in contact with a ligand), and functional epitopes (contact residues that make energetic contributions to binding). Alanine scanning mutagenesis is the trendiest method for mapping functional epitopes because, as alanine substitutions remove side-chain atoms past the β-carbon without introducing additional conformational freedom, they can be used to infer the energetic contributions of individual side-chains to protein binding. As these complexes are of the utmost importance for a rational anticancer therapy development, it is imperative to perform an alanine scanning mutagenesis study that will allow the dissection of the binding free energy in their separate terms, and a more profound knowledge of the fundamental elements that form the hot spot cluster. Here, we apply an improved computational alanine scanning mutagenesis method [19–21], which allows the determination of the hot spots present in both monomers, P53 and MDM2 of the three proteic complexes.

The importance of the hydrogen bonds formed by the protein backbone has been neglected due to the difficulty of quantitatively measuring their contribution to the binding free energy. We also present the computationally calculated binding free energy contribution of the C=O and N–H backbone groups of the interfacial residues of the complex formed between the P53 and the MDM2 proteins.

2 Material and methods

2.1 Model setup

The starting crystallographic structures for the simulations, the complexes formed between the hMDM2 and the P53 protein, between the xMDM2 and the P53 protein, and between the hMDM2 and an optimized P53 protein were taken from the RCSB Protein Data Bank with the PDB entries 1YCR [1], 1YCQ [1], 1T4F [12], and with a resolution of 2.60, 2.30, and 1.90 Å, respectively. A total of 851, 903 and 843 hydrogen atoms were added using the software Protonate from the Amber8 package [22]. The first system comprised a total of 100 amino acids, 15 of which in the P53 protein and 85 in the MDM2 protein. The second complex included a total of 105 amino acids, 17 of which in the P53 protein and 88 in the MDM2 protein. The third contained 97 amino acids, 9 in the

P53 protein, and 88 in the MDM2 protein. All residues were included in their physiological protonation states (charged Glu, Asp, Lys and Arg, all other residues including His were treated as neutral). In the molecular simulations the solvent was modelled through a modified Generalized Born solvation model [23] being the structure first minimized with 1,000 steps of steepest decent followed by 1,000 steps of conjugated gradient to release the bad contacts in the crystallographic structure. Subsequently a 5,000 ps, a 4,000 ps, and a 4,000 ps (MD) simulation were performed starting from the minimized structure for the 1YCR, 1YCQ and 1T4F complexes, respectively. All molecular mechanics simulations presented in this work were carried out using the sander module, implemented in the Amber8 [22] simulations package, with the *Cornell* force field [24]. Bond lengths involving hydrogens were constrained using the SHAKE algorithm [23], and the equations of motion were integrated with a 2 fs timestep being the nonbonded interactions truncated with a 16 Å cutoff. The temperature of the system was regulated by the Langevin thermostat [26–28].

The MM-PBSA script implemented in Amber8 [22] was used to calculate the binding free energies for the complex and for the alanine mutants. The MM-PBSA script [29] was used to perform a post-processing treatment of the complex by using the structure of the complex, and calculating the respective energies for the complex and all interacting monomers. To generate the structure of the alanine mutant complex a simple truncation of the mutated side chain was made, replacing Cγ with a hydrogen atom, and setting the Cβ-H bond direction to that of the former Cβ-C. For the binding free energy calculations, 25 snapshots of the complexes were extracted every 20 ps for the last 500 ps of the run.

2.2 Alanine scanning mutagenesis

The complexation free energy can be calculated using thermodynamic cycle (Scheme 1) where ΔG_{gas} is the interaction free energy between the ligand and the receptor in the gas phase $\Delta G^{\text{lig}}_{\text{solv}}$, $\Delta G^{\text{rec}}_{\text{solv}}$, and $\Delta G^{\text{cpx}}_{\text{solv}}$ are the solvation free energies of the ligand, the receptor and the complex respectively. The binding free energy difference between the mutant and wild type complexes is defined as

$$\Delta\Delta G_{\text{binding}} = \Delta G_{\text{binding}-\text{mutant}} - \Delta G_{\text{binding}-\text{wildtype}} \quad (1)$$

The binding free energy of two molecules is the difference between the free energy of the complex and the respective monomers (the receptor and the ligand):

$$\Delta G_{\text{binding}-\text{molecule}} = G_{\text{complex}} - (G_{\text{receptor}} + G_{\text{ligand}}) \quad (2)$$

The free energy of the complex and respective monomers can be calculated by summing the internal energy (bond, angle and dihedral), the electrostatic and the van der Waals interactions, the free energy of polar solvation, the free energy of nonpolar solvation and the entropic contributions for the molecule free energy:

$$G_{\text{molecule}} = E_{\text{internal}} + E_{\text{electrostatic}} + E_{\text{vdw}} + G_{\text{polar solvation}} + G_{\text{nonpolar solvation}} - \text{TS} \quad (3)$$

The first three terms were calculated using the *Cornell* force field [24] with no cutoff. The electrostatic solvation free energy was calculated by solving the Poisson-Boltzmann equation with the software Delphi v.4 [30,31], using the same methodology of previous works which has been shown in an earlier work to constitute a good compromise between accuracy and computing time [32]. For the energy calculations four internal dielectric constant values, exclusively characteristic of the mutated amino acids were used: 2 for the non-polar amino acids (except Tryptophan), 3 for the polar residues, 4 for the charged amino acids and histidine, and 8 for the Tryptophan residue [20,21]. Recalling that we used only one trajectory for the computational energy analyses, it is important to highlight that side chain reorientation is not included explicitly in the formalism. As amino acid polarity increases, the structural effect beyond the neighbour residues also increases, and the conformational reorganization after alanine mutagenesis should be more extensive. This effect can be mimicked with the use of a set of four different internal dielectric values.

The nonpolar contribution to solvation free energy due to van der Waals interactions between the solute and the solvent and cavity formation was modelled as a term that is dependent on the solvent accessible surface area of the molecule. It was estimated using an empirical relation: $\Delta G_{\text{nonpolar}} = \sigma A + \beta$, where A is the solvent-accessible surface area that was estimated using the Molsurf program, which is based on the idea primarily developed by Michael Connolly [33]. σ and β are empirical constants and the values used were 0.00542 kcal Å^{-2}mol^{-1} and 0.92 kcal mol^{-1} respectively, as this calculation is combined with polar contributions calculated by Delphi. Different values could be used, such as 0.0072 kcal Å^{-2}mol^{-1} and 0 kcal mol^{-1} if in association with the MGB model, as well as 0.005 kcal Å^{-2}mol^{-1} and 0 kcal mol^{-1} if in association with the vtGB and aoGB models [34].

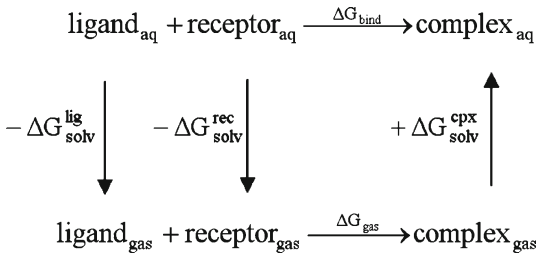

Scheme 1 Thermodynamic cycle used to calculate the complexation free energy

The entropy term, obtained as the sum of translational, rotational, and vibrational components, was not calculated because it was assumed, based on a previous work, that its contribution to $\Delta\Delta G_{\text{binding}}$ is negligible [29].

2.3 Hydrogen bonds at the backbone of the interfacial residues

Hydrogen Bonds are dipole–dipole interactions, which are attributed primarily to partial electrostatic charges in a force-field Hamiltonian. To understand the importance of the hydrogen bonds established by the backbone, we have measured the free binding differences generated upon deletion of the charge of the amide (N–H) and carbonyl (C=O) groups. To ensure electroneutrality we have distributed the remaining charge over the remaining atoms. This procedure was made taking into account the proportions of the contribution of each atom to the final charge of the amino acid residue. It was applied to every single residue at the protein–protein interface previously mutated for an alanine residue. The binding free energy differences were calculated with the MM-PBSA script implemented in Amber8 [22], following Scheme 1 and subsequent equations. Although the use of an internal dielectric value of 2 or 4 did not influence the results significantly, for the energy calculations we have used an internal dielectric constant value of 3 due to the polar nature of the groups in question.

3 Results and discussion

3.1 Alanine scanning mutagenesis study

The improved MM-PBSA method to perform alanine scanning mutagenesis uses the molecular mechanics AMBER force field and a continuum solvation approach with different internal dielectric constant values for different types of amino acid residues. The different internal dielectric constants account for the different degree of relaxation of the interface when different types of amino acids are mutated for alanine; the stronger the interactions these amino acids establish, the more extensive the relaxation should be, and the greater the internal dielectric constant value must be to mimic these effects.

First, to assess the quality of the simulations, we have to make sure that equilibrium has been achieved. Thus, we have plotted in Fig. 2 the root mean square deviations (RMSD) for the backbone atoms of the three complexes (1YCR, 1YCQ and 1T4F) for the production MD simulation (the last 500 ps). As we can see the MD simulations are very stable with RMSD values lower than 2.0, 3.0 or 2.0 for the complexes 1YCR, 1YCQ and 1T4F, respectively.

Table 1 summarizes the results of the computational alanine scanning mutagenesis study of the protein–protein complex 1YCR. To fully understand the binding free energy between hMDM2 and the P53 proteins we present all the individual energy contributions to the relative binding free energy: the electrostatic energy $\Delta\Delta E_{\text{electrostatic}}$, the van der Waals energy $\Delta\Delta E_{\text{vdW}}$, the free energy of nonpolar solvation $\Delta\Delta G_{\text{non-polar solvation}}$, the free energy of polar solvation $\Delta\Delta G_{\text{polar solvation}}$ and the binding free energy difference $\Delta\Delta G_{\text{binding}}$ between the mutant and wild type complexes for all the mutated residues.

Alanine scanning mutagenesis is a valuable procedure for both hot spot detection and analysis of a wide range of protein–protein interfaces because it allows the calculation of the energetic contributions of the individual side-chains to the protein binding.

Botteger et al. [14] have experimentally analysed the P53 protein in the P53:hMDM2 and detected qualitatively a triad of hot spots (Phe19, Trp23 and Leu26). All the other residues of the P53 protein were characterized as null spots [15], meaning that they are less important for complex formation. By inspection of Table 1 it can be observed that we have correctly identified the hot and the null spots present in the P53 protein. It is not possible to make a mathematical analysis of the success rate of the method here due to the lack of quantitative data. Alanine mutation of Phe19 or Trp23 results in the abolishing of the complex binding [15]. This fact justifies the high $\Delta\Delta G_{\text{binding}}$ values calculated for these two residues. We have extended the scanning mutagenesis study to all the residues of the protein-protein interface.

On the hMDM2 protein we have found only one amino acid residue with a binding free energy upon alanine mutation higher than 2.0 kcal mol^{-1} (2.72 kcal mol^{-1}), the Val93 residue. It is obvious that this complex has a highly hydrophobic interface being the $\Delta\Delta E_{\text{vdW}}+\Delta\Delta G_{\text{nonpolar solvation}}$ the main contributors to the $\Delta\Delta G_{\text{binding}}$. The three hot spots in the P53 protein (Phe19, Trp23, Leu26) present $\Delta\Delta E_{\text{vdW}}$ values of 8.71, 12.7 and 2.60 kcal mol^{-1} respectively. These values are the highest values for this energy contribution in the hMDM2 monomer. The hot spot in the hMDM2 protein (Val93) presents a $\Delta\Delta E_{\text{vdW}}$ value of 3.26 kcal mol^{-1} which again is the highest value for this factor in the hMDM2 monomer. As we have previously reported, in the complexes with small interfaces the occlusion of the hot spots from the solvent is made by the formation of a hydrophobic pocket. In this case, the hydrophobic pocket is constituted by these four non-polar amino acid residues that show a high complementarity.

The same study was performed in the complex formed between the P53 and the xMDM2 proteins. Table 2 summarizes the results of the computational alanine scanning mutagenesis study of the protein–protein complex 1YCQ. For this complex the triad of hot spots was again correctly detected. However, we have noticed the presence of a higher

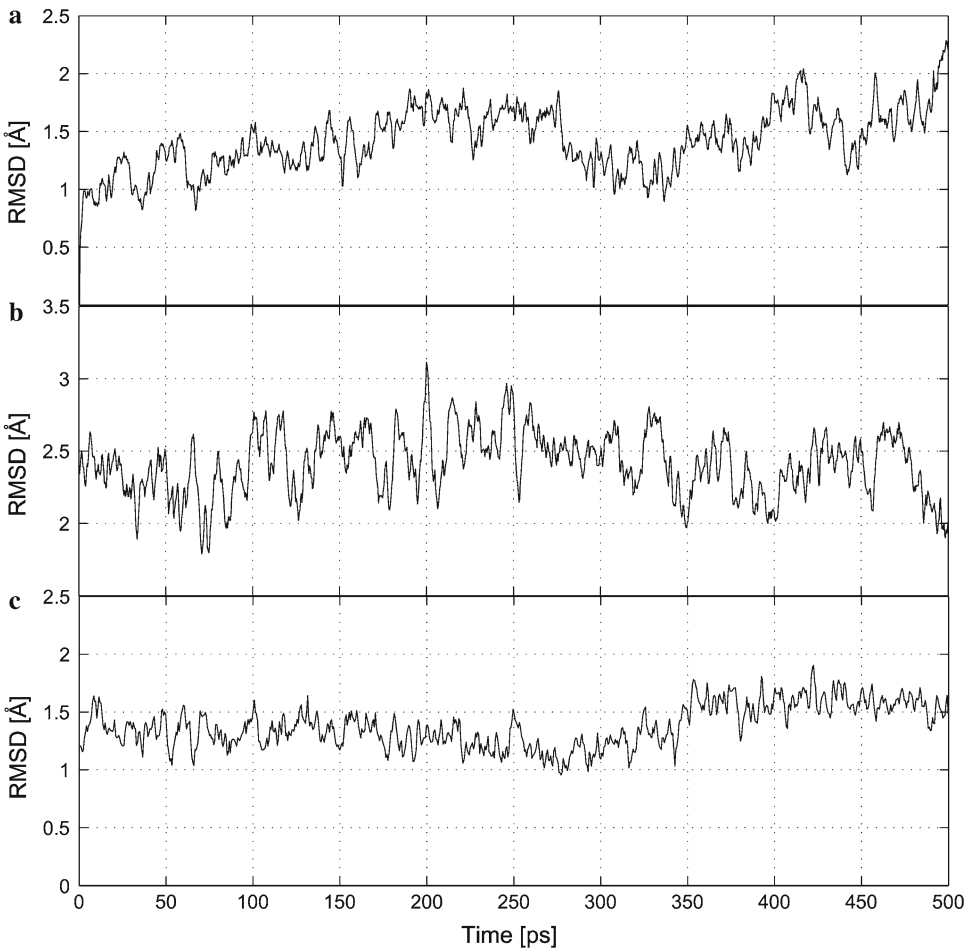

Fig. 2 RMSD plots for the protein backbone of the complex formed **a** the between the hMDM2 and the P53 proteins, **b** the complex formed between the xMDM2 and the P53 proteins, and **c** hMDM2 and an optimized P53 protein relative to its initial structure

Table 1 All the energies are in kcal mol^{-1}

Mutation		$\Delta\Delta E_{electrostatic}$	$\Delta\Delta E_{vdW}$	$\Delta\Delta G_{nonpolar\ solvation}$	$\Delta\Delta G_{polar\ solvation}$	$\Delta\Delta G_{binding}$	$\Delta\Delta G_{exp}$
P53	Thr18Ala	0.33	0.46	0.04	−0.56	0.28	<2.00
	Phe19Ala	−0.68	8.71	0.44	−4.39	4.10	>2.00
	Ser20Ala	1.68	0.21	0.05	−1.24	0.71	<2.00
	Asp21Ala	22.54	0.15	0.00	−22.05	0.65	<2.00
	Leu22Ala	0.08	2.41	0.24	−0.95	1.79	<2.00
	Trp23Ala	0.24	12.7	0.91	−1.54	12.32	>2.00
	His24Ala	−24.13	2.37	0.23	22.58	1.06	<2.00
	Leu25Ala	−0.04	0.85	0.07	−0.33	0.56	<2.00
	Leu26Ala	−0.08	2.6	0.35	−0.88	2.00	>2.00
hMDM2	Leu54Ala	−0.04	3.03	0.09	−3.10	−0.02	NA
	Leu57Ala	−0.04	0.75	−0.03	−0.65	0.04	NA
	Ile61Ala	0.09	1.75	−0.05	−1.02	0.79	NA
	Met62Ala	0.11	2.52	0.18	−1.63	1.18	NA
	Tyr67Ala	0.02	0.42	0.00	−0.31	0.14	NA
	Gln72Ala	0.45	1.03	0.10	−1.03	0.55	NA
	Val93Ala	−0.02	3.26	0.06	−0.59	2.72	NA
	Ile99Ala	−0.14	1.46	−0.02	−0.93	0.38	NA

NA not available

Table 2 All the energies are in kcal mol^{-1}

Mutation		$\Delta\Delta E_{electrostatic}$	$\Delta\Delta E_{vdW}$	$\Delta\Delta G_{nonpolar\ solvation}$	$\Delta\Delta G_{polar\ solvation}$	$\Delta\Delta G_{binding}$	$\Delta\Delta G_{exp}$
P53	Thr18Ala	0.14	0.46	0.05	−0.34	0.32	<2.0
	Phe19Ala	0.00	8.83	0.36	−4.51	4.68	>2.0
	Ser20Ala	−0.22	0.54	0.06	−0.17	0.22	<2.0
	Asp21Ala	6.44	0.06	0.00	−6.50	−0.01	<2.0
	Leu22Ala	−0.03	2.25	0.23	−0.86	1.58	<2.0
	Trp23Ala	0.40	11.89	0.66	−0.95	12.00	>2.0
	His24Ala	−9.26	0.56	0.07	8.75	0.12	<2.0
	Leu25Ala	0.04	0.98	0.08	−0.33	0.77	<2.0
	Leu26Ala	0.14	4.15	0.22	−1.41	3.10	>2.0
xMDM2	Ile50Ala	0.94	2.00	0.12	−0.88	2.18	NA
	Leu53Ala	0.02	0.88	−0.04	−0.07	0.79	NA
	Ile57Ala	0.18	2.13	−0.07	0.16	2.39	NA
	Met58Ala	0.61	2.57	0.27	−1.82	1.63	NA
	Tyr63Ala	−0.12	2.63	0.06	−0.54	2.04	NA
	Gln68Ala	−0.05	0.97	0.15	−0.21	0.87	NA
	Val89Ala	−0.25	2.74	0.09	−0.82	1.75	NA
	His90Ala	6.41	0.34	0.04	−5.83	0.96	NA

NA not available

number of residues with a hot spot character at the xMDM2 monomer. Thus, we have the Ile50, Ile57 and Tyr63 residues with a $\Delta\Delta G_{binding}$ value of 2.19 2.39 and 2.04 kcal mol^{-1} against the −0.02, 0.79 and 0.14 kcal mol^{-1} detected for Leu54, Ile61 and Tyr 67 of the 1YCR complex. For the residue Val89 present in the 1YCQ complex we estimated a value of 1.75, which is almost 1 kcal mol^{-1} lower than the value calculated for Val93 of the 1YCR complex. Figure 3 represents a superimposition of a snapshot of the MD simulation of the 1YCR and 1YCQ complexes. This figure illustrates and justifies the findings mentioned above. As it can be observed Phe19 and Trp23 in the 1YCQ complex are oriented and closer to the Ile61/Ile57 and Tyr67/Tyr63 residues creating more powerful interactions than in the 1YCR complex. Ile50 of the xMDM2 protein is a conservative mutation, which was replaced by Leu54 in the human enzyme along the residues that are in contact with P53. As it can be seen in Fig. 3 and by inspection of Tables 1 and 2, in the 1YCQ complex this residue have an increase contact surface and establishes more important interactions, which are responsible for its warm spot character. Even the hot spot Leu26 of the P53 protein is deeper in the hot spot cluster in the 1YCQ complex justifying a binding free energy 1 kcal mol^{-1} higher than in the 1YCR complex. By contrast, the two hot spots of the P53 protein are less orientated to the Val93/Val89 residue in the 1YCQ complex than in the 1YCR.

Grasberger et al. in 2005 [12] have published a X-ray crystallographic structure of a complex formed between a 9mer peptide (RFMDYWEGL) and the hMDM2 protein. We have

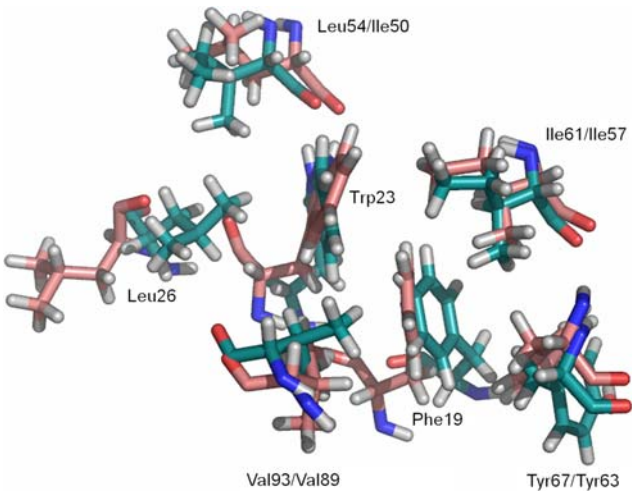

Fig. 3 Superimposing of the 1YCR and 1YCQ complexes. In *pink* we have the 1YCR and in *blue* the 1YCQ (a representative MD snapshot)

performed an alanine scanning mutagenesis study on this complex, and the results are presented in Table 3. First, it is important to mention that the two terminal amino acid residues of the P53 mimic were not subjected to the study because they present an elevated drifting during the MD simulation due to the reduce size of the P53 monomer.

Upon Ser20Met, Leu22Tyr and His24Glu mutagenesis in the P53 protein analogue new hot spots have emerged. This way, we can observe that Met20, Tyr22 present a $\Delta\Delta G_{binding}$ value of 3.49 and 3.66 kcal mol^{-1} respectively. As these

Table 3 All the energies are in kcal mol^{-1}

Mutation		$\Delta\Delta E_{electrostatic}$	$\Delta\Delta E_{vdW}$	$\Delta\Delta G_{nonpolar\ solvation}$	$\Delta\Delta G_{polar\ solvation}$	$\Delta\Delta G_{binding}$	$\Delta\Delta G_{exp}$
P53	Phe19Ala	0.21	6.57	0.61	−3.77	3.64	NA
	Met20Ala	0.15	4.13	0.34	−1.12	3.49	NA
	Asp21Ala	22.83	0.13	0.00	−25.39	−2.42	NA
	Tyr22Ala	−0.99	5.94	0.46	−1.76	3.66	NA
	Trp23Ala	0.13	12.61	0.67	−1.31	12.10	NA
	Glu24Ala	22.14	0.77	0.07	−24.92	−1.93	NA
hMDM2	Leu54Ala	−0.12	2.72	−0.02	−3.21	−0.61	NA
	Leu57Ala	−0.02	0.27	−0.01	−0.27	−0.02	NA
	Ile61Ala	0.28	1.70	−0.15	−0.47	1.38	NA
	Met62Ala	0.27	2.45	0.22	−0.51	2.43	NA
	Tyr67Ala	−0.12	0.93	−0.09	−0.22	0.50	NA
	Gln72Ala	0.14	0.32	−0.06	−0.22	0.19	NA
	Val93Ala	0.09	2.07	0.07	−0.55	1.69	NA
	Ile99Ala	−0.01	0.08	−0.02	0.01	0.06	NA

NA not available

residues present high $\Delta\Delta E_{vdW+}\Delta\Delta G_{nonpolar\ solvation}$ values, the importance of the van der Waals interactions was once more emphasized. In the hMDM2 protein, Val93 still presents a quasi hot spot character as already verified for 1YCQ complex. However, a new hot spot was detected; the Met62 with a $\Delta\Delta G_{binding}$ value of 2.43 kcal mol^{-1}. Figure 4 represents a molecular perspective of a representative MD snapshot of the 1T4F complex. There is a more pronounced packing of the residues capable of hydrophobic interactions (Phe19, Tyr22, Trp23, Tyr63) in comparison to the 1YCR complex increasing the binding affinity between the two monomers. There is also an approximation between the two residues Met62 of the hMDM2 protein and Met20 of the P53 protein, which justifies their hot spot character.

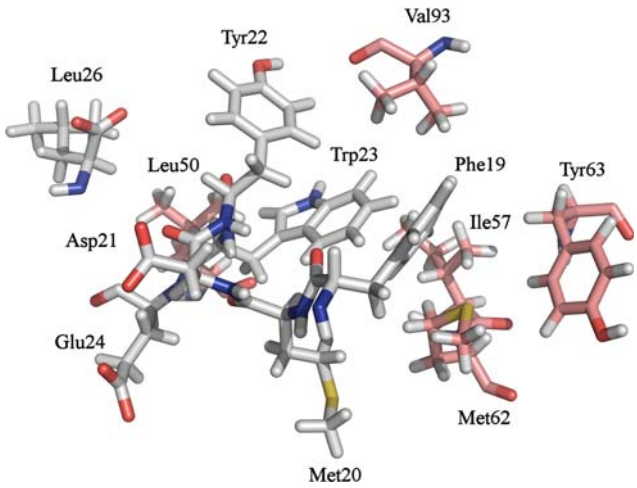

Fig. 4 Molecular representation of the 1T4F complex. In *pink* we have the hMDM2 monomer and in *white* the P53 monomer (a representative MD snapshot)

3.2 Hydrogen bonds at the backbone of the interfacial residues

Although inter-chain interfacial hydrogen bonds are generally weaker than the intra-chain ones they play an important role in binding [35]. We have applied the methodological approach to calculate the binding free energy associated with a main chain hydrogen bond described in the Methods section to the complexes between the P53 and the MDM2 protein. The results attained for the 1YCR complex are presented in Table 4. As we are only considering the electrostatic effect, the $\Delta\Delta E_{vdW}$ and the $\Delta\Delta G_{nonpolar\ solvation}$ are both null.

By inspection of Table 4 we can observe that all the $\Delta\Delta G_{binding}$ values are very small. We only have to emphasize the contribution of the N–H and C=O groups of the residue Leu54, which upon charge deletion generates a $\Delta\Delta G_{binding}$ of 1.85 kcal mol^{-1}. The HE1 atom of the hot spot Trp23 establishes a hydrogen bond with the O atom of the residue Leu54. This is the only intermolecular bond established in this complex, and the distance between the two interacting atoms in function of time for the last 500 ps of the MD simulation is plotted in Fig. 5.

The same study was again made for the complex between the P53 and xMDM2 protein, and the results are presented in Table 5. Ile50 is the residue that presents the highest $\Delta\Delta G_{binding}$ value (2.37 kcal mol^{-1}) because it establishes a hydrogen bond with the HE1 atom of the Trp23 residue. This interaction, which is very important for complex binding, is maintained constant and under a 2.0 Å value during the MD simulation as can be observed in Fig. 6.

Although in the 1YCR the same effect can be found, by examination of Table 5 we can note that Ile57 and Met58

Table 4 All the energies are in kcal mol^{-1}

Protein	Residue	$\Delta\Delta E_{electrostatic}$	$\Delta\Delta G_{polar}$	$\Delta\Delta G_{binding}$
P53	Thr18Ala	1.35	−1.62	−0.27
	Phe19Ala	1.52	−1.81	−0.29
	Ser20Ala	1.97	−1.71	0.26
	Asp21Ala	0.66	−0.72	−0.05
	Leu22Ala	1.2	−1.13	0.09
	Trp23Ala	0.92	−2.22	−1.29
	His24Ala	0.28	−0.75	−0.47
	Leu25Ala	0.26	−1.11	−0.84
	Leu26Ala	−0.25	0.09	−0.16
hMDM2	Leu54Ala	2.46	−1.2	1.27
	Leu57Ala	0.12	−0.14	−0.01
	Ile61Ala	0.23	−0.15	0.09
	Met62Ala	−0.23	0.33	0.1
	Tyr67Ala	−0.14	0.21	0.08
	Gln72Ala	−0.46	−0.67	−1.12
	Val93Ala	−1.37	1.06	−0.31
	Ile99Ala	0.9	−0.63	0.28

Table 5 All the energies are in kcal mol^{-1}

Protein	Residue	$\Delta\Delta E_{electrostatic}$	$\Delta\Delta G_{polar}$	$\Delta\Delta G_{binding}$
P53	Thr18Ala	0.61	−1.13	−0.52
	Phe19Ala	1.28	−1.64	−0.35
	Ser20Ala	0.93	−1.03	−0.10
	Asp21Ala	0.68	−0.84	−0.15
	Leu22Ala	1.06	−1.18	−0.12
	Trp23Ala	0.80	−1.09	−0.28
	His24Ala	0.47	−0.65	−0.18
	Leu25Ala	0.36	−0.16	0.20
	Leu26Ala	0.75	−0.42	0.34
xMDM2	Ile50Ala	2.94	−1.33	1.62
	Leu53Ala	0.34	−0.30	0.05
	Ile57Ala	0.57	−0.22	0.36
	Met58Ala	−0.18	0.44	0.27
	Tyr63Ala	−0.19	0.33	0.15
	Gln68Ala	−0.06	−1.35	−1.40
	Val89Ala	−0.81	0.31	−0.49
	His90Ala	0.02	0.13	0.16

present a $\Delta\Delta G_{binding}$ value of 0.36 and 0.27 kcal mol^{-1} respectively. These values can be explained by the presence of NH-pi hydrogen bonds established between those residues and the phenyl ring of Phe19, and are represented in Fig. 7. When the plane formed by the amide group is roughly perpendicular to the aromatic ring and the amino group points towards the aromatic cycle, the interaction is called amino-pi hydrogen bond [36]. Albeit the energetic contribution of a amino-pi hydrogen bond is usually three times lower than the conventional hydrogen bond [36], it still contributes significantly for complex binding. It is especially important for a correct ligand orientation.

An analysis of the backbone importance was also made for the 1T4F complex, and the results are presented in Table 6. In this complex only the NH-pi hydrogen bonds established between the Ile61 and Met62 residues and Phe19 were detected. The hydrogen bond between the O atom of the Leu54 and the HE1 atom of the Trp23 residues was not detected in the last 500 ps of the MD simulation because these two atoms are separated by at least a 5 Å distance (Fig. 8). After 1.2 ns we can observe that the Tyr22 amino acid, which has a high side-chain volume, gets near the other aromatic residues leading to an increase of the distance between Leu54 and Trp23. For the 9mer peptide an increase of its affinity is probably obtained by a closer packing of hydrophobic residues instead of on backbone inter-chain hydrogen bonding.

4 Conclusion

P53 gene is one of the most frequently mutated genes in human cancer and therefore a complete understanding of the P53 protein interaction with the MDM2 protein is of the utmost importance. The P53–MDM2 binding site is mainly coordinated by a triad of hydrophobic and aromatic residues from P53 that insert deep into the hydrophobic cleft of

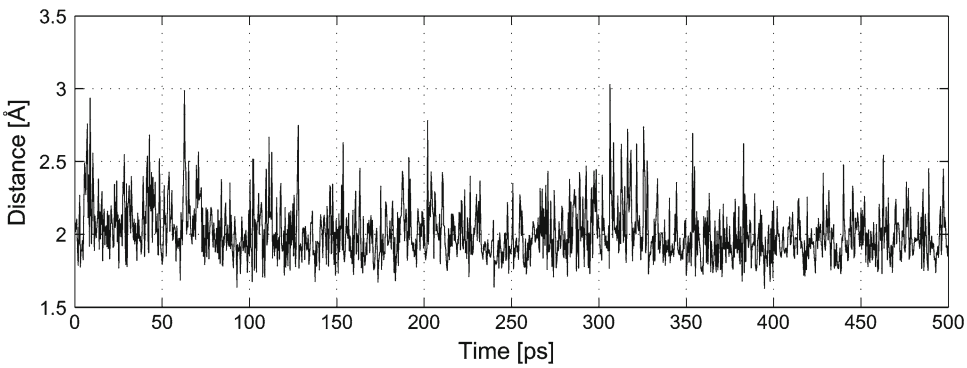

Fig. 5 Distance between the HE1 atom of the hot spot Trp23 and the O atom of the Leu54 residue as a function of simulation time

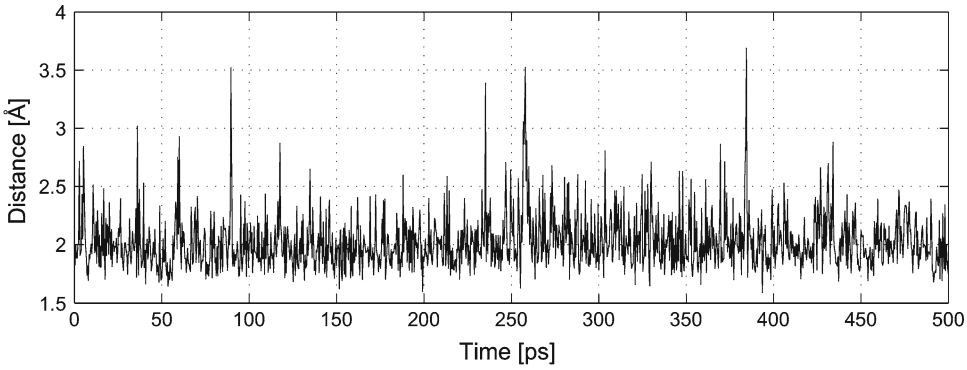

Fig. 6 Distance between the HE1 atom of the hot spot Trp23 and the O atom of the Ile50 residue as a function of MD simulation time

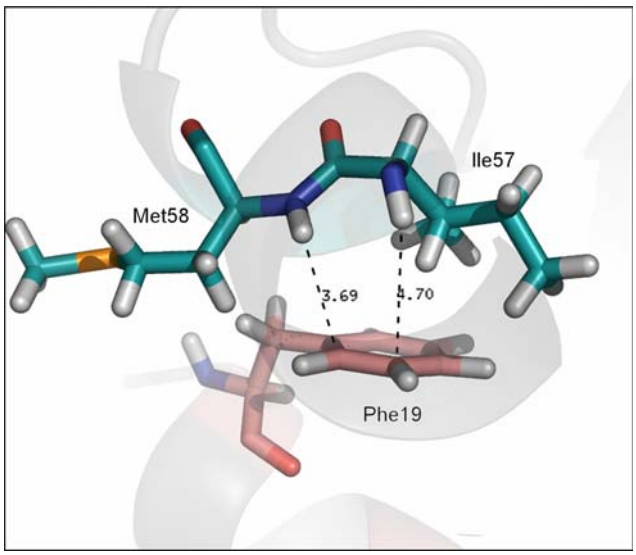

Fig. 7 Molecular perspective of the NH-pi hydrogen bonds established between the Ile57 and Met58 residues and Phe19

Table 6 All the energies are in kcal mol^{-1}

Protein	Residue	$\Delta\Delta E_{\text{electrostatic}}$	$\Delta\Delta G_{\text{polar}}$	$\Delta\Delta G_{\text{binding}}$
P53	Phe19Ala	1.22	−1.58	−0.37
	Met20Ala	1.28	−1.39	−0.11
	Asp21Ala	1.50	−1.77	−0.27
	Tyr22Ala	2.62	−3.13	−0.51
	Trp23Ala	1.39	−2.89	−1.50
	Glu24Ala	3.43	−3.87	−0.44
xMDM2	Leu54Ala	1.90	−1.74	0.15
	Leu57Ala	1.92	−1.73	0.18
	Ile61Ala	0.73	−0.31	0.41
	Met62Ala	0.30	0.01	0.30
	Tyr67Ala	−0.25	0.30	0.04
	Gln72Ala	−0.56	−0.16	−0.72
	Val93Ala	−1.43	0.95	−0.48
	Ile99Ala	0.43	−0.48	−0.05

MDM2. This triad is composed of Phe19, Trp23, and Leu26. We have performed a computational alanine scanning mutagenesis study, which has allowed the decomposition of the binding free energy in its components and the observation that van der Waals interactions are the main force for complex formation. We have observed that the three complexes present some differences in the number and composition of the hot spots. The 1T4F complex presents new hot spot residues, namely the Met20 and Tyr22 amino acids. However the His94Glu mutation does not seem favourable, and thus for the construction of a good P53 mimic peptide it should be avoided.

The importance of the hydrogen bonds formed by the protein backbone has been neglected due to the difficulty of quantitatively measuring their contribution to the binding free energy. In this study we have presented a study of the contribution to the binding free energy of the C =O and N–H groups of the backbone of the P53 and MDM2 proteins. We have to emphasise the presence of a hydrogen bond in the 1YCR complex of on average 2.3 Å between the HE1 atom of the hot spot Trp23 and the O atom of the residue Leu54. This is the only intermolecular bond established in this complex. The same bond was detected in the 1YCQ complex with an average 2.4 Å distance. Ile61/Ile57 and Met62/Met58 of the three complexes present high $\Delta\Delta G_{\text{binding}}$ values that can be explained by the presence of NH-pi hydrogen bonds established between those residues and the phenyl ring of Phe19. Albeit the energetic contribution of an amino-pi hydrogen bond is usually three times lower than the conventional hydrogen bond, it is especially important for a correct ligand orientation.

For the 1T4F complex the amino-pi hydrogen bond was detected but the inter-chain hydrogen bond does not keep stable during the MD simulation. This fact can be explained due to the presence of the Leu22Tyr mutation that increased the hydrophobic character of the protein–protein interface. During the MD simulation the introduction of a group with elevated volume complicates the approximation of the HE1 atom of the hot spot Trp23 and the O atom of the residue Leu54.

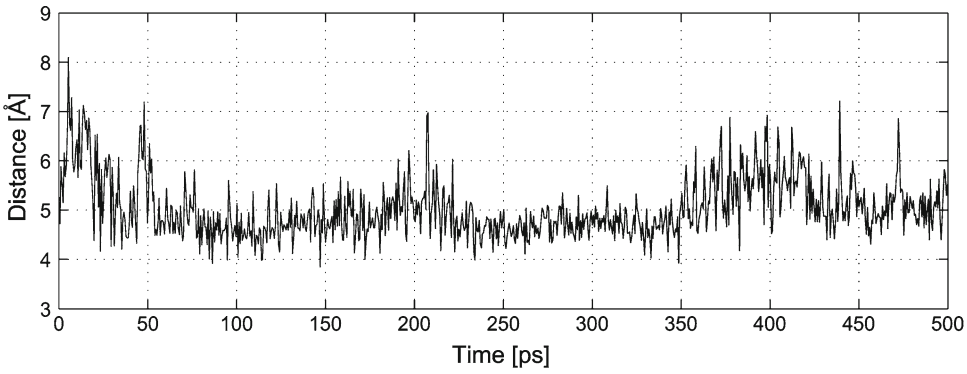

Fig. 8 Distance between the HE1 atom of the hot spot Trp23 and the O atom of the Leu54 residue as a function of simulation time

This study not only shows the reliability of the computational mutagenesis method to detect hot spots but also demonstrates an excellent correlation between the quantitative calculated binding free energy contribution of the C=O and N–H backbone groups of the interfacial residues and the qualitative values expected for this kind of polar interaction. A structural justification was found for every energetic value obtained. An experimental validation is difficult due to the inaccessibility of the backbone. It is important to stress that the latter do not exist because there is no experimental method which can presently evaluate them. In contrast, it is straightforward to calculate the contribution of the backbone to the $\Delta\Delta G_{\text{binding}}$, using our improved computational methodology. It is also important to highlight that the contribution of the backbone to the $\Delta\Delta G_{\text{binding}}$ is smaller than was speculated in the past, which can be explained by the small dimension and number of interactomic interactions established by a dipole N–H or C=O in comparison to a side chain. The energy of the hydrogen bonding interaction depends also on the specific environment of the H-bonds and the degree of spatial and directional complementarity.

Hence, this study opens the possibility of a complete computational predictive analysis of a wide variety of protein-protein complexes.

References

1. Kussie PH, Gorina S, Marechal V, Elenbaas B, Moreau J, Levine AJ, Pavletich NP (1996) Science 274:948–953
2. Chène P (2004) Mol Cancer Res 2:20–28
3. Soussi T, Dehouche K, Beroud C (2000) Hum Mutat 2:105–213
4. Chi CW, Lee SH, Do-Hyoung K, Min-Jung A, Jae-Sung K, Jin-Young W, Takuya T, Masatsune K, Kyou-Hoon H (2005) J Biol Chem 280:38795–38802
5. Welburn JPI, Endicott JA (2005) Sem Cell Devel Biol 16:369–381
6. Mateu MG, Fersht A (1998) EMBO J 17:2748–2758
7. Picksley SM, Lane DP (1993) Bioessays 2:689–690
8. Wu X, Bayle JH, Olson D, Levine AJ (1993) Genes Dev 2:1126–1132
9. Momand J, Zambetti GP, Olson DC, George D, Levine AJ (1992) Cell 2:1237–1245
10. Zhong H, Carlson HA (2005) Proteins 58:222–234
11. Lu F, Chi SW, kim DH, Han KH, kuntz ID, Guy RK (2006) J Comb Chem 8:315–325
12. Grasberger BL, Schubert C, Koblish HK, Carver TE, Franks CF, Zhao SY, Lu T, LaFrance LV, Parks DJ (2005) J Med Chem 48:909–912
13. Massova M, Kollman PA (1999) J Am Chem Soc 121:36
14. Bottger A, Bottger V, Garcia-Echeverria C, Chene P, Hochkeppel HK, Sampson W, Ang K, Howard SF, Picksley SM, Lane DP (1997) J Mol Biol 269:744–756
15. Ma B, Nussinov R (2207) Curr Top Med Chem 7:999–1005
16. DeLano WL, Ultsch MH, de Vos AM, Wells JA (2000) Science 287:1279–1283
17. Bogan AA, Thorn KS (1998) J Mol Biol 280:1–9
18. Ma B, Wolfson HJ, Nussinov R (2001) Curr Opin Struct Biol 11:364–369
19. Moreira IS, Fernandes PA, Ramos MJ (2006) Proteins 63:811–21
20. Moreira IS, Fernandes PA, Ramos MJ (2006) J Phys Chem B 110:10962–10969
21. Moreira IS, Fernandes PA, Ramos MJ (2007) 117:99–113
22. Case DA, Darden TA, Cheatham III TE, Simmerling CL, Wang J, Duke RE, Luo R, Merz HM, Wang B, Pearlman DA, Crowley M, Brozell S, Tsui V, Gohlke H, Mongan J, Hornak V, Cui G, Beroza P, Schafmeister C, Caldwell JW, Ross WS, Kollman PA (2004) AMBER 8, University of California, San Francisco
23. Tsui V, Case DA (2001) Biopolymers (Nucl Acid Sci) 56:275–291
24. Cornell WD, Cieplak P, Bayly CI, Gould IR, Merz KM Jr, Ferguson DM, Spellmeyer DC, Fox T, Caldwell JW, Kollman PA (1995) J Am Chem Soc 117:5179–5197
25. Ryckaert JP, Ciccotti G, Berendsen HJ (1977) J Comput Phys 23:327–335
26. Pastor RW, Brooks BR, Szabo A (1988) Mol Phys 65:1409–1419
27. Loncharich RJ, Brooks BR, Pastor RW (1992) Biopolymers 32:523–535
28. Izaguirre JA, Catarello DP, Wozniak JM, Skeel RD (2001) J Chem Phys 114:2090–2098
29. Huo S, Massova I, Kollman PA (2002) J Comput Chem 23:15–27
30. Rocchia W, Sridharan S, Nicholls A, Alexov E, Chiabrera A, Honig B (2002) J Comp Chem 23:128–137
31. Rocchia W, Alexov E, Honig B (2001) J Phys Chem B 105:6507–6514
32. Moreira IS, Fernandes PA, Ramos MJ (2005) J Mol Struct (Theochem) 729:11–18
33. Connolly ML (1983) J Appl Cryst 16:548–558
34. Gohlke H, Case DA (2004) J Comput Chem 25:238–250
35. Xu D, Tsai CJ, Nussinov R (1997) Protein Eng 10:999–1012
36. Biot C, Buisine E, Kwasigroch JM, Wintiens R, Rooman M (2002) 277:40816–40822